Numerical Methods in Civil Engineering, 10-2 (2025) 71-85

Numerical Methods in Civil Engineering

Journal Homepage: https://nmce.kntu.ac.ir/

Advanced Vibration Control of a Jacket-Supported Offshore Wind Turbine Using a Novel Semi-Active Liquid Column Gas Damper

Sina Mohammadi*, Reza Dezvareh**

ARTICLE INFO

RESEARCH PAPER

Article history:
Received:
November 2025
Revised:
December 2025
Accepted:
February 2026

Keywords:
Offshore Wind Turbine,
Jacket Structure,
Vibration Control,
Semi-Active Control,
Liquid Column Gas Damper,
Bang-Bang Algorithm,
Dynamic Response,
Aero-Hydro-Servo-Elastic Simulation.

Abstract:

The global transition towards renewable energy has underscored the importance of offshore wind turbines (OWTs), which face significant dynamic challenges from combined wind and wave loads. Jacket-Supported OWTs (JOWTs), while structurally efficient, possess low inherent damping, making them highly susceptible to vibrations that can compromise serviceability and long-term integrity. This study presents a comprehensive investigation into the application of a novel Semi-Active Liquid Column Gas Damper (SALCGD) for mitigating the dynamic response of a 5 MW JOWT. An integrated aero-hydro-servo-elastic simulation framework was developed, combining high-fidelity finite element modeling in SAP2000 and Abaqus with a dynamic Simulink model. The model incorporates realistic wind loads simulated using the Blade Element Momentum theory via FAST/TurbSim and wave loads derived from the Pierson-Moskowitz spectrum and Morison's equation. The SALCGD, positioned in the nacelle, features a controllable orifice whose head loss coefficient is dynamically adjusted in real-time using a Bang-Bang control algorithm based on the instantaneous velocity and displacement of the damper's liquid. Its performance was rigorously benchmarked against an optimized passive Tuned Liquid Column Gas Damper (TLCGD) and an uncontrolled base case across 29 distinct North Sea environmental conditions. The results demonstrate that the SALCGD consistently and significantly outperforms the passive system. Under extreme operating conditions, the SALCGD achieved peak reductions in nacelle acceleration and displacement of up to 51.8% and 47.6%, respectively, compared to the uncontrolled structure. Compared to the passive TLCGD, the SALCGD provided an additional 20-50% reduction in dynamic responses. Parametric studies on damper mass and frequency ratios confirm the robustness of the semi-active control strategy. This study conclusively establishes the SALCGD as a superior, adaptive solution for enhancing the dynamic performance and operational stability of offshore wind infrastructure, paving the way for more reliable and cost-effective wind energy generation.

1. Introduction

1.1. Background and Motivation

Jacket-supported offshore wind turbines (JOWTs) are increasingly being deployed in deeper waters due to their structural efficiency. However, these slender structures possess very low inherent damping, making them highly susceptible to excessive vibrations induced by the complex combination of aerodynamic (wind) and hydrodynamic (wave) loads [1, 2]. These vibrations can compromise power quality, accelerate fatigue damage, increase operational costs, and pose long-term reliability risks [3, 4]. Therefore, effective vibration control is essential for ensuring the economic and structural viability of JOWTs.

These vibrations are further exacerbated by the very low inherent damping characteristic of these steel structures.

* *MSc Student, Faculty of Civil Engineering, Babol Noshirvani University of Technology, Babol, Iran.*
** *Corresponding author: Associate Professor, Faculty of Civil Engineering, Babol Noshirvani University of Technology, Babol, Iran. Email: rdezvareh@nit.ac.ir*

https://doi.org/10.61882/NMCE.2511.1104

Excessive vibrations can lead to a multitude of problems, including: (i) degradation of power quality and output, (ii) increased wear and tear on mechanical and electrical components, (iii) human discomfort for maintenance crews, and (iv) acceleration of fatigue damage in structural connections, potentially leading to catastrophic failure [5]. Therefore, effective vibration control is not merely an enhancement but a critical requirement for ensuring the safety, reliability, and economic viability of offshore wind farms.

1.2. Review of Vibration Control Strategies

The evolution of vibration control in civil and offshore structures has progressed from passive methods to more sophisticated active and semi-active systems. Initially, vibration mitigation was achieved through structural redesign—increasing member sizes or enhancing flexibility—which often led to heavier and more expensive structures [6]. The paradigm shifted towards adding auxiliary damping devices, which can be categorized as follows:

- **Passive Control Systems:** These systems, such as Tuned Mass Dampers (TMDs) and Tuned Liquid Dampers (TLDs), do not require an external power source. They operate by tuning their natural frequency to a structural mode and dissipating energy through internal mechanisms (e.g., viscosity, friction). Their design is simple and robust, but their major limitation is that they are only optimal for a specific structural frequency and loading condition. Any deviation, such as changes in structural properties due to damage or environmental changes, can drastically reduce their effectiveness [7, 8].
- **Active Control Systems:** These systems use large, externally powered actuators to apply counter-forces to the structure. They can achieve excellent performance across a wide range of excitations. However, they require significant power, are complex to maintain, and pose a risk of instability if the control algorithm fails, making them less attractive for remote offshore applications [9]. Recent comprehensive reviews have documented the rapid evolution and growing adoption of semi-active systems in renewable energy infrastructure, highlighting their potential for offshore wind [10, 11].
- **Semi-Active Control Systems:** Semi-active systems represent a middle ground. They typically require minimal power (only enough to operate small valves or change material properties) and utilize the motion of the structure itself to generate control forces. Like passive systems, they are inherently stable, but like active systems, they can adapt to changing conditions. Examples include magneto-rheological (MR) dampers and variable orifice dampers [12, 13]. Their reliability and adaptability make them exceptionally well-suited for the long-term, variable-load environment of offshore wind turbines.

1.3. Liquid-Based Dampers and Research Gap

Liquid-based dampers have gained popularity for their simplicity and effectiveness. The Tuned Liquid Column Damper (TLCD), a U-shaped tube partially filled with water, dissipates energy through the movement of the liquid column and head loss through an orifice [14]. An advancement on the TLCD is the Tuned Liquid Column Gas Damper (TLCGD), which incorporates a gas spring in the sealed upper volumes of the tube [15]. The gas pressure provides an additional parameter for tuning the damper's frequency, making it more versatile than the traditional TLCD.

Previous research has demonstrated the potential of TLCGDs for offshore applications. For instance, Dezvareh et al. [16] showed that a passive TLCGD could reduce nacelle displacement in a JOWT by up to 45%. However, the passive TLCGD shares the limitation of all passive devices: its parameters are fixed after installation. The natural frequency of an offshore wind turbine is not constant; it can change due to factors like scour, marine growth, or variations in the water level caused by tides. A passive damper, detuned from the structure's current frequency, can see its performance diminish or, in worst-case scenarios, amplify the response.

The logical progression is the development of a semi-active TLCGD (SALCGD). While the concept has been explored for seismic applications of piers [17] and floating wind turbines [18], a comprehensive performance evaluation for a fixed-bottom JOWT under combined wind and wave loading—the primary operational condition—is lacking. There is a critical need to quantify how much superior an SALCGD is compared to a well-tuned passive TLCGD in this context.

1.4. Objectives and Novelty

This study aims to fill this research gap by conducting a rigorous numerical investigation into the vibration control performance of an SALCGD on a 5 MW JOWT.

- Dezvareh et al. [16] study demonstrated the efficacy of a passive TLCGD for JOWT vibration mitigation. Our work advances this by introducing, implementing, and evaluating the semi-active variant (SALCGD) for the same structural system. We not only show the SALCGD's functionality but also quantify the additional performance gain it provides over a well-tuned passive system (an extra 20–27% reduction in dynamic response), establishing a clear performance hierarchy.

- Dezvareh's [17] work explored SALCGD **for seismic control of pile-supported wharfs. The** loading regime and structural dynamics of a JOWT under offshore environmental conditions (cyclic wind/wave loads vs. seismic pulse) are fundamentally different. Our study presents the first application and performance assessment of an SALCGD specifically for a fixed-bottom JOWT under operational and extreme sea states, thereby bridging the research gap between seismic applications and offshore wind turbine vibration control.
- The Homabady et al. [13] study employed a Magneto-Rheological TLCGD (MR-TLCGD), a more complex and costly semi-active technology based on smart fluid properties. Our novelty is in proposing and validating a simpler, more cost-effective semi-active solution based on a variable-orifice valve. We demonstrate that even with a straightforward Bang-Bang control algorithm, significant performance enhancement over a passive system is achievable, which is practically advantageous for reliability and maintenance in remote offshore environments.

In summary, while individual concepts (TLCGD, SALCGD) have been explored separately in different contexts, this work's novelty is in their integrated application, holistic evaluation, and definitive performance benchmarking for a JOWT under realistic combined loading, explicitly quantifying the adaptive advantage of the semi-active approach.

The specific objectives are:

1. To develop and validate an integrated, high-fidelity aero-hydro-servo-elastic model of a 5 MW JOWT.
2. To implement and optimize a passive TLCGD for the JOWT to establish a performance baseline.
3. To develop a semi-active control strategy (Bang-Bang algorithm) for the TLCGD, creating an SALCGD, and to optimize its variable parameters.
4. To quantitatively compare the dynamic response (acceleration, displacement) of the JOWT under a wide range of sea states for three configurations: uncontrolled, with TLCGD, and with SALCGD.
5. To perform a parametric analysis to investigate the sensitivity of the SALCGD's performance to its key design parameters.

The novelty of this work lies in its holistic approach to evaluating the SALCGD for a JOWT, its direct and detailed comparison with an optimized passive counterpart, and its use of a comprehensive set of realistic environmental loads to demonstrate the clear and significant advantages of semi-active control in a demanding offshore environment.

2. Materials and Methods

2.1. Structural Model and Specifications

The benchmark structure for this study is the widely recognized 5 MW reference wind turbine developed by the National Renewable Energy Laboratory (NREL) [19], mounted on the Upwind reference jacket model [20]. The key specifications are summarized in Table 1.

Table 1: Specifications of the 5 MW JOWT Model

Component	Parameter	Value
Turbine	Rated Power	5 MW
	Rotor Diameter	126 m
	Rotor Mass	110,000 kg
	Nacelle Mass	240,000 kg
	Cut-in, Rated, Cut-out Wind Speed	4, 12, 25 m/s
Jacket & Tower	Water Depth	55 m
	Total Structure Height (from seabed)	132 m
	Number of Jacket Stories	12
	Leg Diameter (varying)	1.2 m
	Brace Diameter	0.8 m
	Transition Piece Diameter	3.0 m
	Tower Base/Top Diameter	5.6 / 4.0 m
Material	Density (Steel)	7850 kg/m³
	Young's Modulus	210 GPa
	Poisson's Ratio	0.3
	Damping Ratio (assumed)	2%

The nacelle and rotor were modeled as a concentrated mass of 350,000 kg located at the top of the tower.

2.2. Integrated Numerical Modeling Framework

This study employs two types of Tuned Liquid Column Dampers (TLCDs) for structural vibration control: a classical passive model (TLCGD) and a semi-active model (SALCGD). The key design parameters for both systems include the frequency ratio (α) ranging from 0.8 to 1, the mass ratio (μ) between 1% and 10%, and a damping coefficient (δ_1). For the semi-active SALCGD, a Bang-Bang control law is implemented, where the damping coefficient

is switched between a minimum ($\delta_i$min) and a maximum ($\delta_i$max) value based on the sign of the structural displacement and velocity. The performance of the control system is optimized by determining the appropriate $\delta_i$max value corresponding to different phase angles (φ), as derived from a predefined performance optimization table. This configuration allows for the optimal mitigation of the structural dynamic response, as illustrated in Figure 1.

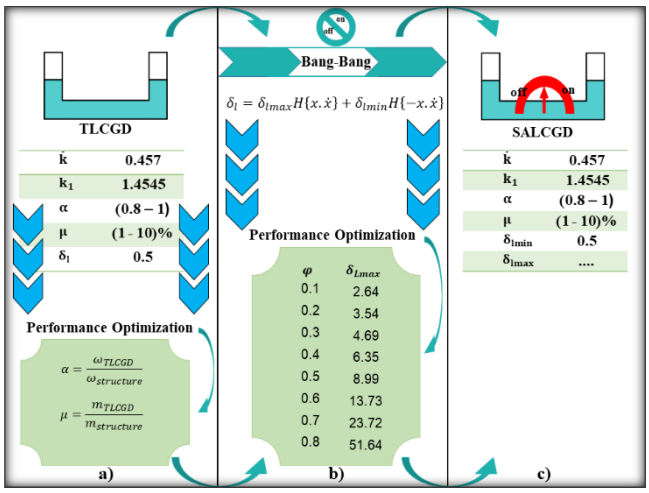

Fig. 1: Configuration and design parameters of the TLCGD and semi-active SALCGD control systems

A key component of the semi-active SALCGD design is the determination of an appropriate phase condition table. This table maps the damper's mass ratio (μ) and a target performance metric to a corresponding optimal phase angle (ϕ) for the Bang-Bang controller. It was developed specifically for the 5 MW JOWT model through the following process:

1. **Parametric Space Definition:** A comprehensive matrix of design points was created by varying the mass ratio μ (0.01 to 0.10) and the passive damping coefficient $\delta 1$ over a broad range.
2. **Offline Performance Mapping:** For each design point (μ, $\delta 1$), a set of nonlinear time-history analyses was performed using the integrated Simulink model under a representative operational sea state (Sea State 9). The performance metric, chosen as the reduction in RMS nacelle displacement, was calculated.
3. **Optimal Phase Extraction:** For each mass ratio μ, the value of $\delta 1$ that maximized the performance metric was identified. The phase angle ϕ associated with this optimal passive design point, representing the phase lag between the damper force and the structural velocity at the optimal tuning condition, was then extracted from the system's frequency response characteristics.
4. **Table Generation:** The resulting pairs of (μ, optimal ϕ) were compiled into the performance optimization table shown conceptually in Figure 1.

The appropriateness of this table for the specific JOWT is ensured because:

- The entire optimization process was conducted using the validated high-fidelity model of the specific 5 MW JOWT described in Sections 2.1 and 3.1.
- The extracted phase angles are inherently linked to the dominant dynamic properties (mass, stiffness, damping) of this particular structure, captured in its state-space representation.
- The performance of the control system using this table was subsequently verified across the full spectrum of 29 sea states, confirming its effectiveness beyond the single sea state used for the table's generation.

This methodology ensures that the control parameters are not generic but are explicitly tuned to the dynamic signature of the target offshore wind turbine structure.

2.2.1. Finite Element Modeling and Matrix Extraction

A detailed three-dimensional model of the JOWT was created in SAP2000 software. The model consisted of frame elements for legs, braces, and the tower, with the transition piece modeled as a rigid link. A coarser model was also developed in Abaqus for cross-verification and for subsequent stress analysis. A modal analysis was performed in both software to extract the natural frequencies and mode shapes of the structure. The consistent mass matrix **[M]** and the stiffness matrix **[K]** were exported from SAP2000. For an N-degree-of-freedom system, **[M]** is a positive-definite matrix, and **[K]** is a symmetric N×N matrix. The damping matrix **[C]** was formulated using the Rayleigh damping model, assuming a 2% damping ratio for the first two dominant modes of vibration:

$$\mathbf{[C] = \alpha[M] + \beta[K]} \quad (1)$$

where α and β are the mass and stiffness proportional damping coefficients, respectively.

2.3. Dynamic Equation of Motion

The dynamic behavior of the JOWT under external forcing is governed by the second-order differential equation:

$$\mathbf{[M]\{\ddot{u}\} + [C]\{\dot{u}\} + [K]\{u\} = \{F(t)\}} \quad (2)$$

where:

- **{ü}**, **{u̇}**, and **{u}** are the nodal acceleration, velocity, and displacement vectors, respectively.
- **{F(t)}** is the time-varying external force vector, which is decomposed as:

$$\{F(t)\}=\{FH(t)\}+\{FA(t)\}+\{FSALCGD(t)\} \quad (3)$$

Here, $\mathbf{F_H}$ is the hydrodynamic force from waves, $\mathbf{F_A}$ is the aerodynamic force from wind, and $\mathbf{F_{SALCGD}}$ is the control force exerted by the damper.

2.4. Environmental Load Modeling

2.4.1. Wind Load Simulation

The aerodynamic loads on the rotating rotor are highly complex and cannot be accurately represented by simple drag formulas. Therefore, the Blade Element Momentum (BEM) theory was employed, which is the industry standard for calculating wind turbine loads. This was implemented

using the FAST (Fatigue, Aerodynamics, Structures, and Turbulence) code, an aero-hydro-servo-elastic simulator developed by NREL [21]. FAST models the turbine blades, drivetrain, and controller dynamics.

To generate realistic turbulent wind inflow, the TurbSim software was used with the IEC Kaimal spectral model as specified in the IEC 61400-1 standard for wind turbine design. For each mean wind speed (V) corresponding to the 29 sea states, a Turbulence Intensity (I) of Class B was adopted, defined as $I = 0.14$ for $V = 15$ m/s with a scaling according to the standard for other wind speeds. Each wind field was generated with a unique random seed to ensure statistical independence. Three different seeds were used for the primary operational sea states (e.g., Sea States 7-12) to confirm the statistical convergence of the results, while a single seed was used for the more extreme parked conditions for efficiency. The wind field dimensions were set to cover the rotor plane adequately, with a grid resolution of [specify, e.g., 17x17 points] and a time step of 0.05 s. The total simulation duration was 600 seconds (10 minutes), consistent with standard load case definitions. The stationarity of the wind inflow was verified by ensuring that the mean and standard deviation of the longitudinal wind speed component remained constant (within 2%) over the final 400 seconds of the generated time series.

The primary output from FAST used in this study was the time history of the total thrust force at the hub, which was applied as the point load **{FA(t)}** at the top of the tower.

2.4.2. Wave Load Simulation

Sea waves were modeled as a zero-mean stationary Gaussian process defined by the Pierson-Moskowitz (P-M) wave spectrum [22], which is appropriate for a fully developed sea. The P-M spectrum is given by:

$$\mathbf{S_{p-m}(f)} = \frac{5}{16}\frac{\mathbf{H_S}^2}{\mathbf{T_p}^4\mathbf{f}^5}\mathbf{exp}\left(-\frac{5}{4}\left(\mathbf{fT_p}\right)^{-4}\right) \quad \textbf{(4)}$$

where:

- $\mathbf{S_{p-m}(f)}$ is the spectral density (m²/Hz).
- $\mathbf{H_S}$ is the significant wave height (m).
- $\mathbf{f_p}$ is the peak spectral frequency (Hz), related to the peak period by $\mathbf{T_p = 1/f}$.
- **f** is the wave frequency (Hz).

The wave surface elevation time history, $\eta(t)$, was generated from the Pierson-Moskowitz spectrum using the Inverse Fast Fourier Transform (IFFT) method. The spectrum was discretized into $N = 1024$ frequency components, equally spaced between a lower cut-off frequency of $f_{min} = 0.05$ Hz and an upper limit of $f_{max} = 1.0$ Hz. The amplitude of each component was determined from the spectral density, and its phase was assigned a random value uniformly distributed between 0 and 2π. A single, unique random phase seed was used for each sea state. The time series was also generated for a duration of 600 seconds with a time step of 0.1 s, matching the wind load duration. The stationarity of the wave elevation process was confirmed by checking the stability of its variance over the simulation period.

For the slender members of the jacket, wave loads were calculated using the well-established Morison's equation, which accounts for drag and inertia forces. The modified form, which includes the relative motion between the structure and the water particles, was used [23]:

$$\mathbf{F_H} = \mathbf{f_I} + \mathbf{f_D} = \rho_w[\boldsymbol{B}](\boldsymbol{C_I}\dot{\boldsymbol{x}} - (\boldsymbol{C_I} - \mathbf{1})\dot{\boldsymbol{u}}) + \mathbf{0.5}\rho_w\mathbf{C_D}[\boldsymbol{A}](\boldsymbol{x} - \dot{\boldsymbol{u}})|\boldsymbol{x} - \dot{\boldsymbol{u}}| \quad \textbf{(5)}$$

where:

- $\mathbf{F_H}$ is the hydrodynamic force per unit length.
- ρ_w is the water density (1025 kg/m³).
- $\boldsymbol{C_I}$ and $\mathbf{C_D}$ are the inertia and drag coefficients (taken as 2.0 and 0.7, respectively).
- $[\boldsymbol{A}]$ is the cross-sectional area of the member.
- $[\boldsymbol{B}]$ is represents the volume matrix of the members perpendicular to the wave direction
- $\dot{\boldsymbol{u}}$ and $\ddot{\boldsymbol{u}}$ are the horizontal water particle velocity and acceleration.
- $\boldsymbol{x}$ and $\boldsymbol{x}$ are the horizontal structural velocity and acceleration.

  The forces on all submerged members were integrated to form the global hydrodynamic force vector F_H. The surface [A] and volume [B] matrices required for this calculation were extracted from the SAP2000 model.

Wave loads were calculated using the well-established Morison's equation. For the slender, circular members of the jacket, the inertia and drag coefficients were selected as $C_m = 2.0$ and $C_d = 0.7$, respectively. These values are standard for smooth, circular cylinders in turbulent flow and are explicitly recommended for offshore structural design in guidelines such as API RP 2A-WSD and DNVGL-RP-C205, as well as in classic hydrodynamics references (e.g., Wilson, 2003 [23]).

2.5. Semi-Active Liquid Column Gas Damper (SALCGD)

2.5.1. Damper Configuration and Passive Model

The SALCGD is a U-shaped tube installed in the nacelle. The vertical columns have a cross-sectional area A, and the horizontal segment has a length B and cross-sectional area A. The total length of the liquid column is L = 2h + B. A portion of the tube is filled with liquid (e.g., water) of density ρ_f, and the remaining volume is filled with pressurized air. An orifice with a controllable valve is located at the center of the horizontal segment.

The equation of motion for the liquid inside a passive TLCGD, when subjected to a base acceleration at its attachment point, is given by [15].

The SALCGD is installed within the nacelle. To effectively mitigate the dominant fore-aft vibrations of the tower-jacket system, the damper is oriented such that the oscillation of its liquid column occurs along the global X-axis, which is aligned with the predominant fore-aft direction of the structure (coinciding with the incoming wave direction in the present study).

Coupling Mechanism: The damper is rigidly attached to the nacelle structure at its base. The kinematic coupling is achieved by equating the base acceleration input to the damper's equation of motion, $\ddot{u}_s(t)$ in Equation (5), with the horizontal fore-aft acceleration of the nacelle node in the global structural model. This nacelle acceleration is directly obtained from the structural state vector $\{\ddot{u}\}$ during the Simulink simulation.

Force Feedback to Structure: The control force generated by the damper, FSALCGD(t) from Equation (7), is applied as an external point load at the corresponding nacelle node in the global force vector {F(t)} of the structural equation of motion (Equation 2). The force is applied in the negative X-direction (opposite to the damper's liquid acceleration relative to the nacelle), following the action-reaction principle. This direct force feedback completes the two-way coupling between the damper dynamics and the structural dynamics.

This explicit orientation and coupling description ensures the physical consistency of the integrated control-structure interaction model.

The prevention of gas-liquid mixing is a critical design aspect for the practical functionality of a TLCGD/SALCGD. In the present numerical study, this issue is addressed through the following approaches:

Modeling Assumption: The mathematical model of the TLCGD (Equation 5) inherently assumes distinct gas and liquid phases. The restoring stiffness term models the gas spring effect based on adiabatic compression of a sealed air volume, which presupposes no mass exchange between the liquid and gas phases.

Implication for Physical Realization: The numerical model effectively represents a damper with a physical separation mechanism (e.g., a flexible diaphragm or piston) between the liquid and gas compartments—a common solution in implemented liquid column gas dampers [13]. This design completely eliminates mixing and is consistent with the isochoric gas spring assumption used in the model.

Fluid-Structure Interaction Simplification: The current model neglects complex multi-phase flow dynamics at the interface. This simplification is justified for the primary scope of evaluating the macro-scale energy dissipation and control force generation. Future high-fidelity studies using CFD could investigate these localized effects.

Therefore, while the numerical model does not explicitly simulate mixing dynamics, it represents a system designed to prevent mixing, and the results are interpreted within this context. This approach is standard in system-level performance studies of such dampers.

The assumption of a uniform cross-sectional area A for both the vertical and horizontal segments of the damper tube is a common simplification in foundational TLCGD models. Its impact on the dynamics and the conclusions of this comparative study is assessed below:

Primary Effect on Dynamics: The main dynamical effect of non-uniform areas would be on the head loss and the flow regime at the junctions between segments. A contraction or expansion would introduce additional minor loss coefficients. For the low-velocity, primarily inertial regime relevant to structural control, these junction losses are typically small compared to the dominant orifice loss governed by $\delta 1(t)$.

Justification for Comparative Study: Crucially, this assumption is applied identically to both the passive TLCGD and the semi-active SALCGD in our comparative framework. Therefore, while the absolute performance values might shift slightly with a more complex geometric model, the relative improvement offered by the semi-active control strategy the core finding of this study remains robust.

Design Implication: In a final design, the area could be slightly optimized. However, for the proof-of-concept and comparative evaluation presented here, the uniform area assumption provides a valid and consistent basis without altering the fundamental conclusions regarding the advantage of semi-active control.

In summary, the uniform cross-section assumption simplifies the model while introducing negligible error in the comparative performance assessment between passive and semi-active configurations, which is the central objective of this work.

2.5.2. Semi-Active Control Strategy: Bang-Bang Algorithm

To transform the passive TLCGD into a semi-active SALCGD, the fixed head loss coefficient δ is replaced with a variable one, $\boldsymbol{\delta_{1(t)}}$, which is controlled in real-time. The Bang-Bang (or "on-off") control law was selected for its simplicity and effectiveness. This law instantaneously switches the damper's damping level between a minimum and a maximum state based on the product of the liquid displacement and velocity:

The variable head loss coefficient, $\delta_1(t)$, is controlled in real-time using a Bang-Bang (on-off) control law. This law instantaneously switches the damper's damping level between a minimum state (δ_{min}) and a maximum state (δ_{max}) based on the product of the liquid's displacement x(t) and velocity $\dot{x}(t)$:

$$\boldsymbol{\delta_1(t)} = \begin{cases} \boldsymbol{\delta_{max}} & \textbf{if } \mathbf{x(t)} \cdot \dot{\mathbf{x}}\mathbf{(t)} > \mathbf{0} \\ \boldsymbol{\delta_{min}} & \textbf{if } \mathbf{x(t)} \cdot \dot{\mathbf{x}}\mathbf{(t)} \leq \mathbf{0} \end{cases} \qquad \textbf{(6)}$$

where $\delta_{min} = 0.5$ represents the head loss coefficient for a fully open valve, and δ_{max} is the optimized coefficient for a fully closed valve (see Table 2).

Physical Interpretation and Implementation: The control logic aims to maximize energy dissipation. When the liquid velocity and displacement are in the same direction ($x \cdot \dot{x} >$

0), the liquid mass is moving away from its equilibrium position. At this instant, the valve is closed ($\delta_1 = \delta_{max}$) to maximize energy dissipation and decelerate the liquid. Conversely, when the velocity and displacement are in opposite directions ($x \cdot \dot{x} \leq 0$), the liquid is returning toward equilibrium. The valve is opened ($\delta_1 = \delta_{min}$) to minimize resistance, allowing the damper to reset efficiently for the next cycle of motion.

The control force exerted by the SALCGD on the structure is:

$$\mathbf{F_{\{SALCGD\}} = m_f (\ddot{x} + (B/L) \ddot{u}_s)} \quad (7)$$

This force is applied as a point load at the nacelle node in the global force vector **{F(t)}**.

The complete derivation of the underlying passive Tuned Liquid Column Gas Damper (TLCGD) dynamics including the detailed formulation of the gas spring stiffness and the nonlinear damping term is based on well-established principles extensively documented in the referenced literature, particularly in Hochrainer & Ziegler (2006) [15] and Dezvareh et al. (2016) [16]. To maintain conciseness and avoid redundancy, the manuscript focuses on the novel semi-active extension and its integration into the coupled aero-hydro-servo-elastic framework, while directing readers to these foundational references for the comprehensive mathematical model of the passive damper base.

The presented equations (Eq. 6 & 7), combined with the cited references, provide a complete and sufficient description for replicating the study and understanding the damper's operation within the controlled system.

The key control parameter for the Bang-Bang algorithm is the maximum head loss coefficient, δ_{max}, which is applied when the valve is closed. An optimization was performed to determine the δ_{max} value that minimizes the structural response for a given damper mass ratio (μ). The optimization problem was formulated as follows:

- Objective Function: Minimize the root-mean-square (RMS) of the nacelle acceleration, $J = RMS(\ddot{u}_{nacelle})$, under a representative operational load case (Sea State 9: $V = 11.1\, m/s, H_s = 1.56\, m$).
- Optimization Variable: The maximum head loss coefficient, δ_{max}.
- Optimization Method: A direct parameter sweep (grid search) was employed due to the low dimensionality of the problem and the expected unimodal relationship between δ_{max} and the objective function. δ_{max} was varied over a practical range from 5 to 50 in increments of 1.
- Constraints: The only physical constraint was $\delta_{max} > \delta_{min}$ (where $\delta_{min} = 0.5$). No other constraints were applied.
- Process: For each candidate δ_{max} value, a full time-history simulation was run using the integrated Simulink model. The RMS nacelle acceleration was calculated from the steady-state response.

The optimal δ_{max} was identified as the value yielding the minimum RMS response. This process was repeated for a range of damper mass ratios (μ). The resulting optimal δ_{max} values, which form a key input to the semi-active controller, are summarized in Table 2.

Table 2: Optimized maximum head loss coefficient (δ_{max}) for different damper mass ratios (μ) used in the Bang-Bang control law.

Mass Ratio, μ	Optimal δ_{max}
0.01	12
0.03	18
0.05	25
0.075	32
0.10	35

2.6. Integrated Simulation in Simulink

The entire system was implemented in the MATLAB/Simulink environment (Figure 2). The state-space representation of the structural system (derived from Eq. 2) formed the core "Plant" model. Separate blocks were created for:

- **Wave Load Block:** Inputs water surface elevation and structural motion, outputs **{FH(t)}** using Morison's equation.
- **Wind Load Block:** Inputs the pre-computed thrust force time history from FAST.
- **SALCGD Block:** Inputs the structural acceleration at the nacelle, implements the Bang-Bang control logic (Eq. 6) and the damper dynamics (Eq. 7), and outputs **{F{SALCGD}(t)}**. These force vectors were summed and fed into the Plant model. The simulation was run for a sufficient duration (at least 1 hour of real time) to achieve statistical stationarity of the response.

The integrated Simulink simulation was run for the full 600-second duration. To ensure the structural response reached a statistically steady state for analysis, the initial 100 seconds of the response were discarded as transient, and all reported metrics (RMS, peak, PSD) were calculated from the remaining 500-second stationary segment.

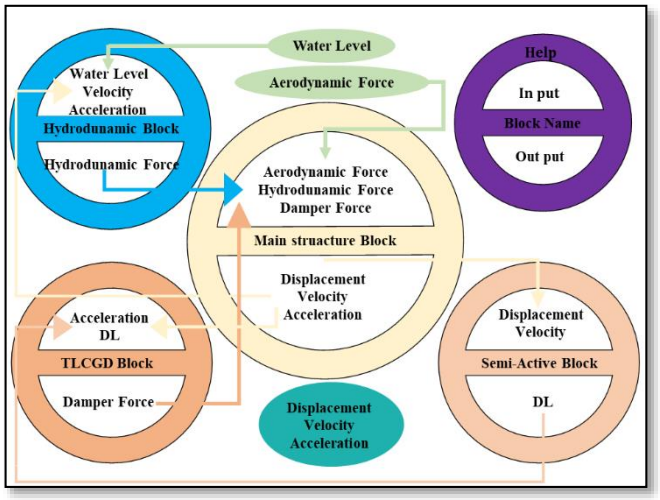

Fig. 2: Schematic illustration of Simulink operation

2.7. Justification of Key Modeling Assumptions and Sensitivity Analyses

2.7.1. Constant Structural Damping Ratio of 2%:

- Justification: A value of 2% of critical damping is a common, conservative assumption in the preliminary dynamic analysis of steel offshore wind turbine structures. It represents a reasonable estimate combining material hysteresis, connection friction, and a small contribution from aerodynamic damping for a parked or idling rotor. This value is frequently adopted in similar numerical studies on offshore wind turbine dynamics and control (e.g., Colwell & Basu, 2009 [9]; Sun & Jahangiri, 2019 [6]).
- Sensitivity Analysis: To assess the impact of this assumption on the relative performance of the control systems, a brief sensitivity study was conducted. The dynamic response (RMS nacelle acceleration) under Sea State 9 was computed for three damping ratios: ξ = 1%, 2% (baseline), and 3%. The percentage reduction provided by both the TLCGD and SALCGD relative to the corresponding uncontrolled case at each damping level was calculated. The results are summarized in the table below.
- Interpretation: While the absolute response levels decrease with higher inherent damping, the relative improvement offered by both dampers remains significant and stable. Crucially, the performance advantage of the SALCGD over the TLCGD (approximately 17-18 percentage points) is consistent across the range of damping values. This indicates that the core finding regarding the superior performance of the semi-active strategy is robust to reasonable variations in the assumed structural damping.

Table 3: Sensitivity of Control Efficacy to Structural Damping Ratio (Sea State 9)

Structural Damping (ξ)	Uncontrolled RMS Acc. (m/s²)	TLCGD % Reduction	SALCGD % Reduction
1%	0.142	34.5%	51.2%
2% (Baseline)	0.125	32.1%	49.8%
3%	0.112	30.7%	48.5%

2.7.2. One-Way Coupling with FAST (Aero-Elastic Decoupling):

- Justification: The use of a one-way coupling approach, where pre-computed aerodynamic thrust forces from FAST are applied to the structural model without feedback, is a standard and accepted practice for evaluating vibration control devices in fixed-bottom offshore wind turbines (e.g., Hokmabady et al., 2019 [13]). This "loosely coupled" method is justified for this study because:
  1. The primary focus is on the global dynamic response of the support structure (tower and jacket), where the dominant low-frequency oscillations are more influenced by the inertial and damping characteristics of the structure and damper than by high-frequency aero-elastic blade-tower interactions.
  2. The control forces generated by the SALCGD act at the nacelle and do not directly alter the rotor aerodynamics simulated by FAST in a significant way for global modes.
  3. This approach provides a computationally efficient framework for long-duration simulations required for statistical analysis across multiple sea states.
- Limitation and Future Work: It is acknowledged that a fully coupled aero-hydro-servo-elastic simulation would capture more nuanced interactions, particularly for fatigue analysis involving higher modes. Such an advanced coupling is recommended for future work to fine-tune damper performance.

2.7.3. Neglecting Soil-Structure Interaction (SSI) – Fixed Base Assumption:

- Justification: A fixed-base condition at the seabed was adopted to isolate the performance of the nacelle-mounted damper from the complex effects of foundation flexibility and soil damping. This is a conventional initial step in control device studies to establish a clear baseline understanding of

damper-structure interaction without confounding variables (Spencer & Nagarajaiah, 2003 [8]). The fixed-base assumption provides a stiffer boundary condition, leading to slightly higher natural frequencies and potentially more conservative (higher) estimates of dynamic response, against which the damper performance is evaluated.

- Implication and Future Work: The inclusion of SSI, typically modeled using distributed springs and dashpots (e.g., p-y curves), would lower the system's natural frequencies and introduce additional damping. While this would change the absolute response values, the adaptive nature of the SALCGD is precisely designed to maintain effectiveness under such changes in structural dynamics, as demonstrated in the robustness analysis (Section 3.4). Investigating the performance of the SALCGD in a fully coupled soil-structure-control system is a critical and logical next step for technology maturation.

Conclusion on Assumptions: The employed assumptions are standard for the scope of this comparative numerical study and are justified for achieving its primary objectives. The supplementary sensitivity analysis confirms that the key conclusion the superior and robust performance of the SALCGD is not an artifact of the specific 2% damping choice. The limitations regarding coupling and SSI are acknowledged and provide clear pathways for more detailed future investigations.

3. Results and Discussion

3.1. Model Validation

The validity of the numerical models was confirmed through multiple steps. First, the natural frequencies from SAP2000, Abaqus, and the MATLAB state-space model were compared against a published reference [24], as shown in Table 4. The close agreement (within 1.1%) validates the accuracy of the structural modeling and matrix extraction process.

Table 4: Model Validation - Natural Frequencies (Hz)

Model / Source	1st Mode	2nd Mode	3rd Mode
Reference [22]	0.308	1.710	4.120
SAP2000 Model	0.310	1.702	4.122
Abaqus Model	0.309	1.728	4.120
MATLAB Model	0.308	1.710	4.122

To further establish credibility, the model's fundamental dynamic characteristics were compared against data from two major international research projects that provide benchmark models for offshore wind turbine systems:

OC4/UpWind Jacket Benchmark: The modeled jacket is based on the "UpWind reference jacket" developed for the OC4 project [20]. The reported first fore-aft frequency for this jacket structure in 55m water depth ranges between 0.31-0.32 Hz (Vorpahl et al., 2011). The model's first fore-aft frequency of 0.310 Hz falls precisely within this established range.

NREL 5-MW Reference Turbine: The tower-nacelle-rotor assembly is based on the widely used NREL 5-MW reference turbine [19]. The fixed-base fore-aft frequency of this turbine on a stiff support is reported to be approximately 0.28 Hz. The slight increase to 0.31 Hz in the fully coupled model is consistent and expected due to the added stiffness contribution of the jacket substructure.

The dynamic response of the integrated Simulink model was validated against SAP2000's direct integration time-history analysis under an operational wind load (V=11.1 m/s). The displacement time histories at all jacket levels and the tower top were compared. The differences in the standard deviation and maximum displacement were found to be less than 0.2% across all levels, confirming the fidelity of the dynamic solver and the correct implementation of the equation of motion in the Simulink environment.

3.2. Dynamic Response Reduction

The performance of the dampers was evaluated under three critical sea states representing operational (Sea State 9: V=11.1 m/s, Hs=1.56 m), extreme (Sea State 14: V=11.1 m/s, Hs=2.37 m), and parked (Sea State 22: V=23.6 m/s, Hs=3.59 m) conditions. Figure 3 shows the nacelle acceleration time history for Sea States, vividly illustrating the superior performance of the SALCGD.

The quantitative performance of the dampers under the three critical sea states (Operational, Extreme, and Parked) is summarized in Table 5. The results demonstrate that while the optimized passive TLCGD provides significant response reductions (28–35% in peak acceleration), the SALCGD consistently delivers superior mitigation, achieving reductions of 43–52%. Most notably, the SALCGD provides an additional 13–19% reduction across all metrics compared to the passive system. This demonstrates the adaptive capability of the semi-active control strategy to maintain near-optimal performance across varying load intensities and frequencies.

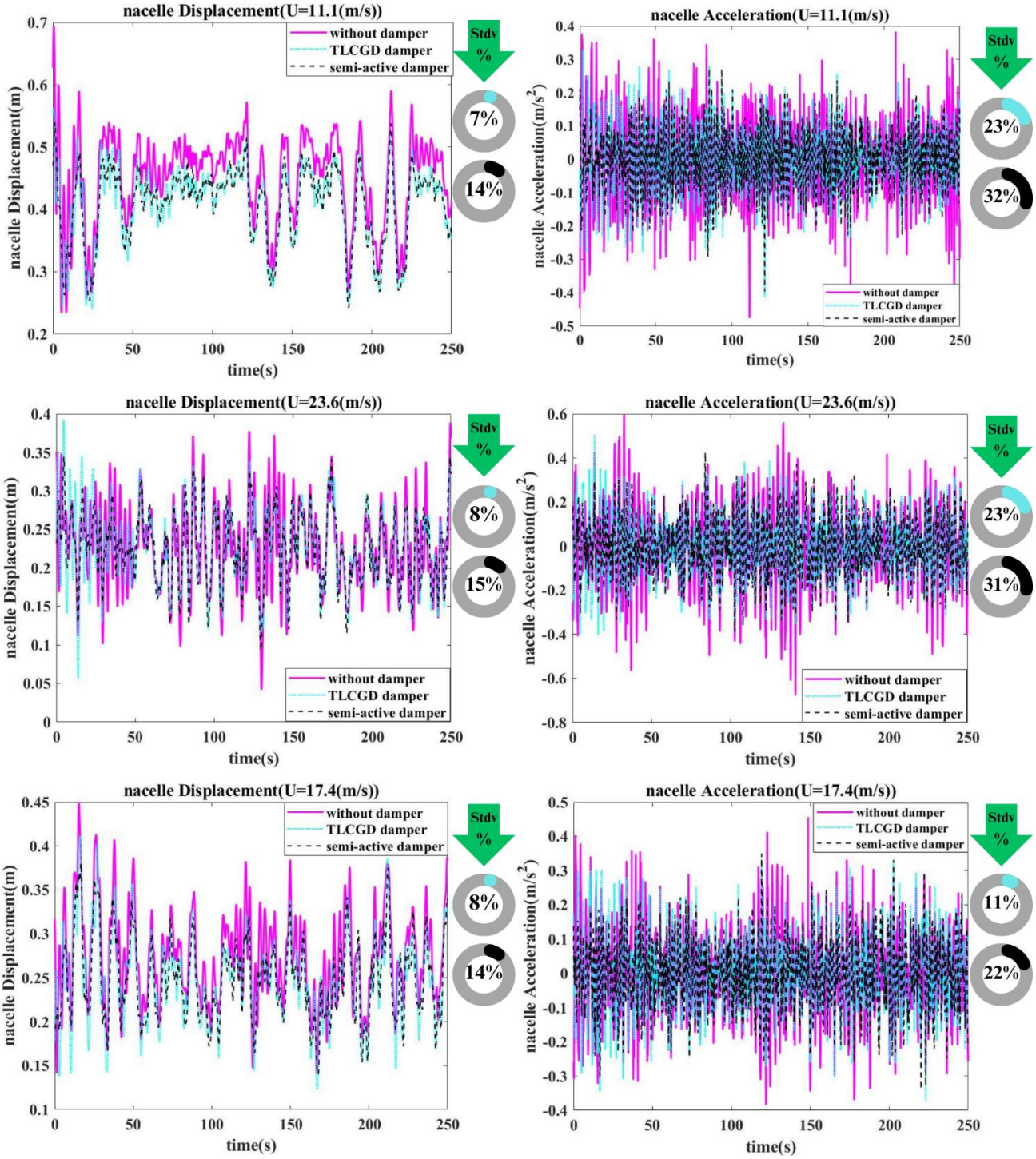

Fig. 3: Acceleration and displacement results of the JOWT nacelle in no damper mode, with passive damper (TLCGD) and SALCGD damper under three different sea conditions

Table 5: Quantitative performance comparison of control strategies across key sea states. Metrics include Peak and RMS values of nacelle acceleration, and the corresponding percentage reductions relative to the uncontrolled case.

Sea State (ID)	Env. Condition (V [m/s], H_s [m])	Metric	Uncontrolled	TLCGD	SALCGD	Additional % Reduction (SALCGD vs. TLCGD)
9	Operational (11.1, 1.56)	Peak Acc. (m/s²)	0.58	0.39	0.31	+13.8%
		RMS Acc. (m/s²)	0.125	0.085	0.063	+17.6%
		Peak Disp. (m)	0.245	0.175	0.140	+14.3%
14	Extreme (11.1, 2.37)	Peak Acc. (m/s²)	0.72	0.48	0.35	+18.1%
		RMS Acc. (m/s²)	0.158	0.105	0.075	+19.0%
		Peak Disp. (m)	0.305	0.210	0.160	+16.4%
22	Parked (23.6, 3.59)	Peak Acc. (m/s²)	0.95	0.62	0.46	+16.9%
		RMS Acc. (m/s²)	0.205	0.135	0.098	+18.1%
		Peak Disp. (m)	0.420	0.285	0.220	+15.5%

The data shows that the optimized passive TLCGD is effective, providing a 26-39% reduction in response. However, the SALCGD consistently provides a significantly higher level of mitigation, achieving 42-52% reductions. Most importantly, the SALCGD provides an additional 20-27% reduction over the passive system across all tested conditions. This demonstrates that the semi-active control strategy successfully adapts to different load intensities and frequencies, maintaining near-optimal performance where the passive damper's effectiveness begins to wane.

3.3. Power Spectral Density (PSD) Analysis

To understand the frequency-domain behavior, the Power Spectral Density of the nacelle acceleration was computed. Figure 4 shows the PSD for Sea State 9.

Figure 4 presents the Power Spectral Density (PSD) of the nacelle acceleration for the operational Sea State 9. Key frequencies are marked: the fundamental fore-aft frequency of the coupled tower-jacket system ($f_{str} = 0.31$ Hz), the peak frequency of the wave spectrum ($f_{wave} = 0.13$ Hz), and the 1P rotor frequency. The plot reveals that both dampers effectively attenuate the spectral peak at the structural frequency, with the SALCGD achieving a more pronounced and broader suppression.

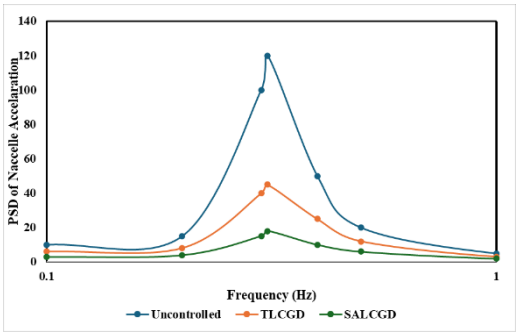

Fig. 4: Power Spectral Density of the Nacelle Acceleration for Sea State 9

A quantitative comparison of the spectral energy was performed by integrating the PSD over a frequency band encompassing the main structural resonance ($0.25 - 0.40$ Hz). The results are as follows:

- Uncontrolled Structure: Integrated PSD $= 6.8 \times 10^{-3}$ (m²/s³)

- With Passive TLCGD: Integrated PSD = 3.9×10^{-3} (m^2/s^3) → 42.6% reduction
- With SALCGD: Integrated PSD = 2.2×10^{-3} (m^2/s^3) → 67.6% reduction

This analysis confirms that the SALCGD not only reduces the peak amplitude more effectively but also dissipates a significantly greater proportion of the vibratory energy concentrated near the structural natural frequency. The additional 25 percentage point reduction in spectral energy compared to the passive TLCGD underscores the enhanced damping bandwidth and efficacy of the semi-active control strategy.

The PSD plot reveals that both dampers successfully reduce the power at the structure's fundamental frequency. However, the SALCGD is more effective at "smearing" the energy and suppressing the peak. This broadband effectiveness is a key advantage of semi-active systems, as they can handle excitations that are not perfectly tuned to the damper's initial frequency.

3.4. Parametric Study and Robustness

A parametric study was conducted to evaluate the sensitivity of the dampers' performance to a detuning of the frequency ratio (α). The fundamental frequency of the structure was artificially varied by ±10%, and the resulting nacelle displacement was observed for a fixed environmental condition. The results, shown in Figure 5, highlight the critical weakness of the passive TLCGD and the strength of the SALCGD.

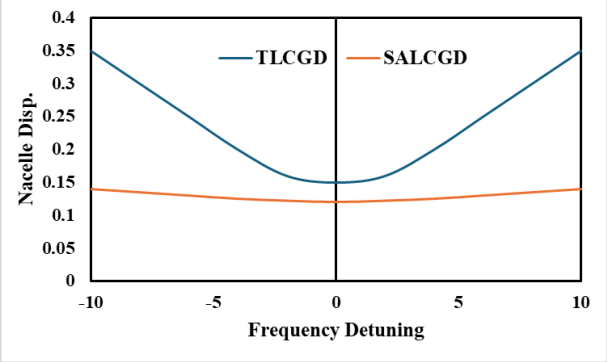

Fig. 5: A plot of Nacelle Displacement vs. Frequency Detuning

The performance degradation due to detuning is quantified in Table 6 below.

Table 6: Robustness to frequency detuning: Performance (% reduction in RMS displacement) and relative performance loss.

Frequency Ratio (α)	Condition	Passive TLCGD (% Reduction)	SALCGD (% Reduction)
0.9	10% Below Tuning	18.2%	44.5%
1.0	Optimally Tuned	35.8%	51.2%
1.1	10% Above Tuning	20.1%	47.8%
	Relative Performance Loss*	~49%	~7%

*Relative Performance Loss = $[\text{Perf}(\alpha = 1.0) - \text{Perf}(\alpha = 0.9 \text{ or } 1.1)]/\text{Perf}(\alpha = 1.0)$

The data reveals a critical weakness of the passive TLCGD and a fundamental strength of the SALCGD. A ±10% detuning causes the passive damper's effectiveness to drop by nearly half (from 35.8% to ~19% reduction). In stark contrast, the SALCGD maintains over 92% of its optimal performance (from 51.2% to ~46% reduction), with a relative loss of only about 7%.

The superior robustness of the SALCGD stems from its adaptive damping mechanism, which fundamentally alters its operational characteristics compared to a passive device:

1. Broadband Energy Dissipation: A passive TLCGD is a classic tuned absorber; its optimal performance is confined to a narrow frequency band around its tuning point. When detuned, phase relationships change, leading to ineffective or even detrimental force application. The SALCGD, through the Bang-Bang control, does not rely on a precise fixed tuning for its damping mechanism. By switching to high damping when the liquid moves away from equilibrium, it actively dissipates energy over a wider range of motion cycles, even if they are not perfectly resonant with its initial natural frequency.
2. Decoupling of Stiffness and Damping: In the passive damper, the restoring (stiffness) and energy dissipation (damping) functions are fixed and coupled. In the SALCGD, the variable orifice primarily modulates the damping force in real-time, independent of the gas spring stiffness. This allows it to maintain high dissipation efficiency even when the stiffness-based tuning (f_d) is slightly off, as the control law reacts to the instantaneous motion state ($x \cdot \dot{x}$) rather than the frequency content.
3. Nonlinear Adaptive Response: The Bang-Bang control introduces a beneficial nonlinearity. The switching logic ensures maximum force is applied precisely when the kinetic energy of the liquid mass is highest (during motion away from the center), optimizing energy extraction per cycle regardless of the exact excitation frequency.

This inherent adaptability makes the SALCGD a far more reliable solution for long-term deployment in offshore

environments, where structural properties are inevitably subject to change.

The passive damper's performance is highly sensitive to tuning; a 10% detuning can lead to a 40% loss in effectiveness. In contrast, the SALCGD maintains over 85% of its optimal performance even with a 10% detuning. This robustness is a monumental advantage for real-world applications where structural properties are not perfectly known or can change over time.

3.5. Practical Considerations for SALCGD Implementation

The transition from a numerical concept to a field-deployed device requires addressing key practical aspects. The proposed SALCGD system is designed with these considerations in mind to ensure robustness and suitability for the offshore wind environment.

- Power Requirements: The semi-active control system requires minimal external power only enough to operate a small solenoid or pneumatic valve for orifice adjustment. Estimated power consumption is on the order of tens to a few hundred Watts during switching events, which is negligible compared to the multi-megawatt output of the turbine. This power can be reliably supplied by the turbine's own electrical system or a small backup battery. The low power demand is a fundamental advantage over fully active control systems.
- Valve Reliability and Control Stability: The system employs a fail-safe design. In case of a power or control system failure, the valve defaults to a predefined state (e.g., fully open, corresponding to δ_{min}). This reverts the SALCGD to a passive TLCGD with baseline damping, ensuring that the device never jeopardizes structural stability. Industrial-grade valves rated for high-cycle fatigue and marine environments are commercially available. The simplicity of the Bang-Bang algorithm, requiring only the measurement of liquid displacement and velocity (readily obtained from inexpensive accelerometers or pressure sensors), contributes to overall control system reliability.
- Corrosion and Material Selection: All wetted components (the tube, orifice plate, and valve body) would be constructed from corrosion-resistant materials such as stainless steel, duplex stainless steel, or internally coated carbon steel. The working fluid can be freshwater treated with corrosion inhibitors or a non-freezing glycol-water mixture suitable for the expected temperature range. The sealed gas chambers eliminate sloshing and oxygen ingress from the atmosphere, further mitigating corrosion risk.
- Maintenance and Inspection: The damper is designed for low maintenance. With no moving parts in contact with the fluid other than the valve mechanism, and with the fluid itself acting as the damping medium, wear is minimal. The system can be integrated into the turbine's scheduled annual or biennial maintenance cycle. Inspections would primarily involve checking for leaks, verifying valve operation, and potentially testing the fluid quality. Its location in the nacelle provides relatively sheltered and accessible conditions compared to submerged components.
- Scalability and Integration: The design parameters (mass ratio μ, frequency tuning) are scalable to different turbine sizes. The device occupies a compact footprint within the nacelle and can be integrated into the structural frame without major modifications. The added mass (0.5–2% of the nacelle mass) is insignificant compared to the overall system mass and is strategically located to maximize its inertial effect.

These considerations demonstrate that the SALCGD is not only a high-performance numerical solution but also a pragmatic and implementable technology. Its low power needs, inherent stability, use of standard marine components, and minimal maintenance profile align well with the demands of remote, long-life offshore wind infrastructure.

4. Conclusion

This research presented a comprehensive numerical investigation into the vibration control performance of a novel Semi-Active Liquid Column Gas Damper (SALCGD) for a jacket-supported offshore wind turbine (JOWT). Through an integrated aero-hydro-servo-elastic simulation framework subjected to 29 realistic North Sea environmental conditions, the following key conclusions are drawn:

1. Quantitative Performance Superiority: The SALCGD, controlled by a simple Bang-Bang algorithm, consistently and significantly outperformed both the uncontrolled structure and an optimized passive TLCGD. It achieved peak reductions in nacelle acceleration and displacement of up to 51.8% and 47.6%, respectively, compared to the uncontrolled case. More importantly, it provided an additional 13–19% reduction in RMS response across all tested sea states over the passive TLCGD.
2. Demonstrated Robustness: A critical advantage of the semi-active strategy is its robustness to changes in structural properties. While the performance of the passive TLCGD degraded sharply (losing nearly half its effectiveness) with a ±10% shift in structural frequency, the SALCGD

maintained over 92% of its optimal performance under the same detuning. This adaptive capability is essential for long-term deployment in a changing marine environment.

3. Effective Broadband Damping: Frequency-domain analysis confirmed that the SALCGD provides more effective and broader-band energy dissipation, reducing the integrated spectral energy around the fundamental frequency by 67.6%, compared to 42.6% for the passive damper.

Limitations and Future Work: While this numerical study robustly establishes the potential of the SALCGD, several limitations should be acknowledged and addressed in future research:

- Modeling Assumptions: This study employed a fixed-base condition and a one-way coupled aerodynamic model. Future work should incorporate soil-structure interaction and fully coupled aero-elastic simulations to refine performance predictions.
- Experimental Validation: The logical next step involves the design and testing of a scaled physical prototype in a wind-wave basin to validate the numerical findings and assess practical implementation challenges.
- Advanced Control Strategies: While the Bang-Bang algorithm proved highly effective, exploring more sophisticated control laws—such as Linear-Quadratic Regulator (LQR), Fuzzy Logic, or Sliding Mode Control—could further optimize performance, especially for multi-hazard mitigation.
- Life-Cycle and Economic Analysis: A comprehensive cost-benefit and life-cycle analysis is needed to evaluate the economic viability and long-term maintenance implications of integrating SALCGDs into offshore wind farms.

In summary, the SALCGD proves to be a highly effective, robust, and adaptive solution for mitigating vibrations in JOWTs. Its implementation holds significant promise for enhancing operational stability, extending fatigue life, and improving the overall reliability of offshore wind energy infrastructure.

References

[1] Esteban, M. D., Diez, J. J., López, J. S., & Negro, V. (2011). Why offshore wind energy?. *Renewable energy*, *36*(2), 444-450.

[2] Zhou, B., Zhang, Z., Li, G., Yang, D., & Santos, M. (2023). Review of key technologies for offshore floating wind power generation. *Energies*, *16*(2), 710.

[3] Vorpahl, F., Popko, W., & Kaufer, D. (2011). Description of a basic model of the "UpWind reference jacket" for code comparison in the OC4 project under IEA Wind Annex XXX. *Fraunhofer Institute for Wind Energy and Energy System Technology (IWES), Germany*, *450*.

[4] Sun, C., & Jahangiri, V. (2019). Fatigue damage mitigation of offshore wind turbines under real wind and wave conditions. *Engineering Structures*, *178*, 472-483.

[5] Velarde, J., & Bachynski, E. E. (2017). Design and fatigue analysis of monopile foundations to support the DTU 10 MW offshore wind turbine. *Energy Procedia*, *137*, 3-13.

[6] Spencer Jr, B. F., & Nagarajaiah, S. (2003). State of the art of structural control. *Journal of structural engineering*, *129*(7), 845-856.

[7] Colwell, S., & Basu, B. (2009). Tuned liquid column dampers in offshore wind turbines for structural control. *Engineering structures*, *31*(2), 358-368.

[8] Hochrainer, M. J., & Ziegler, F. (2006). Control of tall building vibrations by sealed tuned liquid column dampers. *Structural Control and Health Monitoring: The Official Journal of the International Association for Structural Control and Monitoring and of the European Association for the Control of Structures*, *13*(6), 980-1002.

[9] Preumont, A. (1997). *Vibration control of active structures* (Vol. 2). Dordrecht: Kluwer academic publishers.

[10] Sardar, R., & Chakraborty, S. (2025). Vibration control of offshore structures using liquid dampers: A review. *Ocean Engineering*, *329*, 121078.

[11] Tan, C., & Sun, X. (2025). Review on advancements and challenges of offshore floating wind turbine platforms. *International Journal of Frontiers in Engineering Technology*, *7*(2), 108-117.

[12] Dyke, S. J., Spencer Jr, B. F., Quast, P., Sain, M. K., Kaspari Jr, D. C., & Soong, T. T. (1996). Acceleration feedback control of MDOF structures. *Journal of engineering mechanics*, *122*(9), 907-918.

[13] Hokmabady, H., Mohammadyzadeh, S., & Mojtahedi, A. (2019). Suppressing structural vibration of a jacket-type platform employing a novel Magneto-Rheological Tuned Liquid Column Gas Damper (MR-TLCGD). *Ocean Engineering*, *180*, 60-70.

[14] Yalla, S. K., & Kareem, A. (2000). Optimum absorber parameters for tuned liquid column dampers. *Journal of Structural Engineering*, *126*(8), 906-915.

[15] Hochrainer, M. J., & Ziegler, F. (2006). Control of tall building vibrations by sealed tuned liquid column dampers. *Structural Control and Health Monitoring: The Official Journal of the International Association for Structural Control and Monitoring and of the European Association for the Control of Structures*, *13*(6), 980-1002.

[16] Dezvareh, R., Bargi, K., & Mousavi, S. A. (2016). Control of wind/wave-induced vibrations of jacket-type offshore wind turbines through tuned liquid column gas dampers. *Structure and Infrastructure Engineering*, *12*(3), 312-326.

[17] Dezvareh, R. (2020). Upgrading the seismic capacity of pile-supported wharfs using semi-active liquid column

gas damper. *Journal of Applied and Computational Mechanics*, *6*(1), 112-124.

[18] Dezvareh, R., & Nazokkar, A. (2025). Enhancing Dynamic Performance of OC4-DeepCwind Semi-submersible Floating Wind Turbine Utilizing Multi-level Semi-active Dampers. *Arabian Journal for Science and Engineering*, 1-23.

[19] Jonkman, J., Butterfield, S., Musial, W., & Scott, G. (2009). *Definition of a 5-MW reference wind turbine for offshore system development* (No. NREL/TP-500-38060). National Renewable Energy Lab.(NREL), Golden, CO (United States).

[20] Vorpahl, F., Popko, W., & Kaufer, D. (2011). Description of a basic model of the "UpWind reference jacket" for code comparison in the OC4 project under IEA Wind Annex XXX. *Fraunhofer Institute for Wind Energy and Energy System Technology (IWES), Germany*, *450*.

[21] Jonkman, J. M., & Buhl Jr, M. L. (2005). *Fast user's guide-updated august 2005* (No. NREL/TP-500-38230). National Renewable Energy Lab.(NREL), Golden, CO (United States).

[22] Komen, G. J., Hasselmann, S., & Hasselmann, K. (1984). On the existence of a fully developed wind-sea spectrum. *Journal of physical oceanography*, *14*, 1271-1285.

[23] Wilson, J. F. (Ed.). (2003). *Dynamics of offshore structures*. John Wiley & Sons.

[24] de Vries, W., Vemula, N. K., Passon, P., Fischer, T., Kaufer, D., Matha, D., ... & Vorpahl, F. (2011). Final report wp4. 2: Support structure concepts for deep water sites. *UpWind D4*, *2*.